Characterization of Qualified Grid Nodes for the Identification of Power Network Oscillations

Akash Kumar Mandal and Swades De

Abstract—Rapid integration of renewable energy sources and power electronic components in the conventional energy systems has resulted in increased sub-synchronous oscillations (SSOs) in the power network. As a consequence, accurate and exhaustive monitoring of SSOs is critical for reliable system operation. The importance of failure-proof network operation has necessitated the requirement of a revised notion of power system stability and control. In this regard, this paper presents a benchmark study on power grid disturbances to efficiently identify the most qualified buses that should be monitored to capture the perturbations present in the network. Our analysis shows that the proposed approach is computationally much faster and utilizes a significantly reduced number of buses for disturbance identification as compared to the state-of-the-art, without compromising on the disturbance identification accuracy in the network. Theoretical formulation of optimization objectives are verified by the results from the data-driven performance results using phasor measurement units (PMUs). PMU data was generated through real-time structured computer-aided design (RSCAD) simulation. Considering various adversities, such as single PMU loss, single line loss, measurement noise-infested PMU data, and compromised PMU operation, our results demonstrate $\geq 50\%$ and $\geq 75\%$ reduced data footprint under normal and adverse system operations, respectively, while identifying $> 95\%$ of the critical SSO frequencies, with a $> 94\%$ reduced execution time. Also, the proposed approach presents $\approx 25\%$ enhanced accuracy of SSO identification in standard IEEE networks, $\approx 25\%$ improved noise immunity, $\approx 15\%$ additional immunity to grid adversities as compared to the state-of-the-art machine learning and statistical SSO identifiers, with only 0.21% accuracy loss on per-node increase in grid size.

Index Terms—Integer optimization, optimum power grid monitoring, phasor measurement unit (PMU), real-time structured computer-aided design (RSCAD), sub-synchronous oscillation (SSO).

I. INTRODUCTION

With increasing renewable integration in the conventional power network and high voltage direct current transmission technology, the utilization of power electronics-interfaced components has increased manifolds [1]. This has resulted in an increased sub-synchronous and super-synchronous inter-harmonics injected into the power signals, causing sub-synchronous oscillations (SSOs). The origin of SSO can be attributed to the interaction between the inter-harmonics and torsional vibration frequencies of the generator shaft system [2]. These disturbance frequencies propagate to various parts of the system, causing system destabilization and degradation in power quality [3]. Therefore, real-time identification of such

system oscillations is pertinent to the stability and control of modern power networks.

Phasor measurement units (PMUs) serve the purpose of grid health monitoring with densely sampled and time-stamped values of important power system attributes. However, the field data from these real-time Internet-of-Thing (IoT) devices is often infested with power system electromagnetic impairments and allied measurement noise [4]. Furthermore, with the advent of modern communication technologies in the conventional power networks, the abnormalities arising by the virtue of cyber attacks and similar IoT-related adversities has increased manifold [5]. Therefore, for real-time identification of the power network oscillations, it is important to select the most qualified PMUs, so that the data from these devices sufficiently characterize the network instability or SSO conditions.

A. Literature Review and Motivation

The research to date in SSO identification can be broadly divided into two sets. The first set [6], [7] uses modal transformation techniques for SSO detection in the modern power networks. The works in [8] and [9] employed fast Fourier transform, [10] utilized wavelet theory, and [11] used Prony algorithm for generating detailed information about the oscillation modes. However, the accuracy of these methods depend on the data size and its spatial variability. To mitigate such issues, the approach in [12] employed a Taylor-Fourier multi-frequency model-based SSO parameter estimator and [13] utilized a waveform-based method for fast and accurate identification of SSOs. Although, these methods address the issue of higher data footprint, the aspect of co-analysis of multiple node dynamics has not been accounted thus far in the literature. As a result, the accuracy of SSO detection in a power network is compromised with an increase in their operational complexity.

Nodal PMU data-based estimation of SSOs is proposed using the empirical wavelet transform in [14], while the utilization of PMU data in SSO identification in high renewable-injected grids is proposed in [15]. On one hand, it has been established in literature that, the signature from one PMU is not enough to capture the oscillation dynamics of complete power network [16]. On the other hand, using multiple PMU data could be burdensome from communication, data storage, and efficient execution standpoints [17], [18]. Therefore, the identification of the optimum number of PMUs, i.e., the PMUs monitoring the most qualified nodes is important for a computationally light and accurate detection of SSOs [19].

The second type of analysis [20], [21] involves the use of machine learning (ML) approaches in the identification of

A. K. Mandal and S. De are with the Department of Electrical Engineering and Bharti School of Telecommunication, IIT Delhi, New Delhi 110016, India (e-mail: {akash.kumar.mandal, swadesd}@ee.iitd.ac.in). A preliminary version of this work was presented in IEEE International Conference on Energy Technology for Future Grids 2023, Wollongong, Australia.

the power system SSOs. A Data-driven mode identification method was proposed in [22], [23], and a PMU data based power system event detection and classification using unlabeled data is proposed in [24]. The study in [25] used wavelet-based feature extraction from the recorded real-time dataset followed by identification of the class of the disturbance using machine learning. An S-transform-based feature extraction strategy was proposed in [26], followed by an analysis using a combination of extracted features in [27]. The work in [28] used deep learning techniques to perform disturbance classification using an image-converted form of the PMU dataset. In context of the SSO identification, the common learning strategies that have been utilized involve deep neural network, support vector machine, random forest, decision tree, artificial neural network, K-nearest neighbour, and naive Bayes [29].

Although ML has evolved as an effective tool in identification of such real-time events, these strategies often suffer from high computational complexity [30], over-fitting, and local convergence issues [31], and the requirement of a prior data model [32]. Much of these issues arise with the requirement of a huge dataset in any learning-based methodology. Though this helps to reduce modeling error which results in an improved accuracy of classification/identification and faster convergence, it simultaneously leads to the aforementioned trade-offs. The study in [33] proposed a PMU data-based disturbance classification approach considering bad data. However, the research is limited to disturbance classification, relaxing the real-time identification of power network disturbances. Furthermore, the lack of a co-analysis framework makes the wideband disturbance analysis approach in [33] inefficient and complex.

In our preliminary study [34], we proposed a novel optimization framework for the identification of the most qualified buses that can help in capturing the critical SSO frequency components and their mode shapes of the power network. A PMU data-based optimization was used for the experimental validation of the obtained theoretical results. However, the measurements and the system's operating conditions were considered ideal. As an advance, this study considers real system conditions with measurement noise-infested PMU data and re-purposes the data-based optimization in [34] to include the aspect of non-ideal system conditions. As a result, a revised set of optimal power system buses and the most qualified PMUs are obtained. As an exhaustive consideration, this study also considers practical adversities resulting from single PMU loss, single line loss, and other IoT-specific impairments caused by cyber attacks or similar unethical activities.

Remark 1. *It is notable that, the state-of-the-art PMUs only provision a maximum reporting rate up to $200/240$ fps (nominally $25/30$ fps) for $50/60$ Hz grids, respectively. This creates a bottleneck in our analysis in identifying the super-synchronous frequency components. However, the oscillation identification approach proposed in our work is capable of identifying wideband oscillation frequencies (electromechanical to electromagnetic band). Thus, in this work, we have specifically focused on identifying the SSOs for the sake of technological correctness.*

B. Contributions and Significance

The key contributions of this research are as follows:

1) A theoretical system-based optimization problem advocating co-analysis of multiple power grid nodes is formulated for the identification of the important power system buses, that can help in capturing the critical frequency components of the SSO.
2) A mathematical framework of the measurement noise-infested PMU data is developed for the data-based optimization formulation, by proposing a revised spectral decomposition and correlation value, leading to an updated hypotheses threshold.
3) A data-based characterization of the most critical system parameter(s) from the perspective of identifying SSOs in perturbed power networks is undertaken.
4) The solution to the proposed optimization framework is studied using a standard IEEE 5-bus system. The knowledge of the most critical system parameters are utilized in the theoretical optimization, which is solved for IEEE 14, 30, 39, 57, and 118-bus networks, and the results are validated with the PMU data-based optimization problem to capture the disturbance signature for the complete power network.
5) Finally, the optimization problems are revisited considering system adversities resulting from single PMU loss and single line loss conditions. A practical measurement scenario is considered with measurement noise-infested PMU data. Also, as an exhaustive study, the possibility of compromised PMU operation by cyber attacks or similar abnormalities is considered for establishing the validity of the data-based optimization.

Theoretical results corroborated by the real-time structured computer-aided design (RSCAD) simulation verify the appropriateness of the proposed optimization formulation and the observations that are noted as a byproduct. This study helps in establishing a benchmark in defining the most qualified buses, i.e., characterizing the minimum number of system nodes that must be co-analyzed to extract an accurate and exhaustive information about the SSOs. For example, in a 57-bus system, the number of disturbance identification location in the proposed approach reduces from 18 to 8, with a $\approx 96\%$ reduction in the execution time and 94% reduction in time when averaged over all considered test systems. Furthermore, on an average, the proposed SSO identification approach demonstrates $\approx 25\%$ enhanced accuracy of SSO identification in standard IEEE networks, $\approx 25\%$ enhanced noise immunity, $\approx 15\%$ enhanced immunity to grid adversities as compared to the state-of-the-art ML and statistical SSO identifiers, with only 0.21% accuracy loss on per-node increase in grid size.

It is notable that, under adversities such as, single PMU loss, single line loss, noise-impaired PMU data, and compromised PMU operation, the execution time does not vary considerably in the proposed SSO identification approach, while still capturing $> 95\%$ of the disturbance energy for all considered test networks. This suggests that the proposed algorithm converges to the optimum for systems of varied sizes.

TABLE I: List of symbols used in the analysis

x_i	Binary decision variable for the choice of bus i
w_{ij}, α_i, β_{ij}	Importance of jth Eigenvalue of bus i, where $w_{ij} = \alpha_i \beta_{ij}$ α_i: ability of node i to cause oscillation, β_{ij}: contribution of jth eigenmode of ith node in aggregate oscillation
λ_{ij}	jth eigenvalue associated with bus i
$\phi_i^{(m)}$, $\theta_i^{(f)}$	Binary variables representing the presence of mth eigenmode and fth frequency component in the state matrix of bus i
l_i, μ_i, π_i	Binary variables indicating whether PMU installed at ith grid node, whether it is chosen for collaboration, and if it is available or lost
χ_t, χ_0	χ_i-squared test criterion $\chi_t = \sqrt{\sum_{j=1}^{q}(\delta\varphi_{\Delta t}^{(j)} \cdot \sigma_{\varphi_{\Delta t}^{(j)}}^{-1})^2}$ and χ_0 is test threshold level
$a_i^{(m)}$, $b_i^{(f)}$	$a_i^{(m)}$ is a binary variable indicating whether the PMU at node i captures measurements from mode m $b_i^{(f)}$ is a binary variable indicating whether PMU i captures measurements within frequency range f
$\mathbf{U}$, $\boldsymbol{\Sigma}$, $\mathbf{V}$	Upper triangular matrix, matrix of singular values, and lower triangular matrix (in order)
$\kappa_j(\Delta t)$, $\xi_j(\Delta t)$	Defined time sensitivity of jth parameter and the sensitivity of chi-squared metric with the jth parameter
$\Delta\eta_{\text{SOA}}$	Drop in the SSO identification efficiency with unit increase in system node
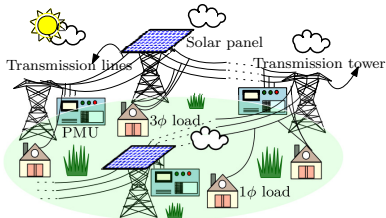
Fig. 1: System model for collaborative oscillation monitoring.

C. Paper Organization

The rest of the paper is organized as follows: Section II describes the system model. Section III presents the formulation of theoretical optimization used in the identification of SSOs in the power network. Section IV formulates its data-based optimization counterpart, wherein the impact of measurement noise is discussed. Finally, the results are presented in Section V, followed by the conclusion in Section VI.

II. SYSTEM MODEL

Schematic representation of a power network is shown in Fig. 1. Let the network has N nodes which are collected in the set $\mathcal{N}$, such that $\|\mathcal{N}\|_c = N$. Here $\|\cdot\|_c$ denotes the cardinality operation. High renewable penetration and increased presence of power electronic components inject SSOs of the form $u(t) = a_0 + \sum_{n=1}^{N} a_n e^{-\sigma_n t}\sin(\omega_n t + \delta_n)$, where a_n, σ, $\omega_n \geq 0$, and δ_n denote the amplitude, damping coefficient, frequency, and initial phase offset of the nth oscillatory component, respectively. The network is designed to supply power to various load types, requiring a good power factor. For the sake of grid health monitoring, the PMUs are placed at strategic positions in the grid, that record data for various important power system features. This data is utilized for the identification of SSOs in the power network.

As a general case, we consider that the PMU data has field-induced measurement noise due to the surrounding electromagnetic radiations from the high voltage lines. Further, the PMUs are considered to communicate data over optical ground wire. As reported in literature [35], we consider the possibility of compromised PMU operation due to cyber attack. Additionally, we consider single PMU loss and single line loss conditions in the grid. The next section formulates

the theoretical optimization for detecting the SSOs in the power network. This theoretical formulation is validated for mathematical correctness using the data-based optimization undertaken in the subsequent sections. The list of mathematical notations used in the manuscript are mentioned in Table I.

III. THEORETICAL OPTIMIZATION FOR DETECTION OF POWER SYSTEM SSO

For the system described in the previous section, let the selection of the ith bus be represented using a binary decision variable $x_i \in \{0,1\}$, $i \in \mathcal{N}$, such that $x_i = 1$ if the ith bus is chosen and 0 otherwise. Then, the selection of the significant power system nodes/buses can be achieved through the following optimization problem:

$$
\begin{aligned}
(\mathbf{P}1): \quad & \max_{x_i} \sum_i x_i r_i \\
\mathbf{C}11: \quad & \sum_i x_i \phi_i^{(m)} \geq 1, \quad \forall m \\
\mathbf{C}12: \quad & \sum_i x_i \theta_i^{(f)} \geq 1, \quad \forall f \in [0, f_s) \\
\mathbf{C}13: \quad & \phi_i^{(m)}, \theta_i^{(f)}, x_i \in \{0,1\}, \quad \forall i, m, f
\end{aligned}
\tag{1}
$$

where $r_i = \sum_{j=1}^{M_i} w_{ij}\lambda_{ij}$, M_i represents the total number of eigenvalues, and λ_{ij} denotes the jth eigenvalue that is associated with bus i. Weights w_{ij} represent the importance assigned to the jth eigenvalue of bus i. $\phi_i^{(m)}$ and $\theta_i^{(f)} \in \{0,1\}$ are binary indicators representing the presence of mth eigenmode and fth frequency component in the state matrix of bus i, where f_s represents the synchronous frequency of the grid.

The maximization in $(\mathbf{P}1)$ operates over x_i to select the most significant power system nodes or buses to capture critical frequency components of SSOs. Constraint $\mathbf{C}11$ ensures that every important mode of SSO in the power network is associated to at least one of the chosen buses. $\mathbf{C}12$ ensures that the fth frequency band of SSO is an eigenfrequency of at least one selected bus. Lastly, $\mathbf{C}13$ imposes a binary limit on all the relevant variables.

A. Definition of $\phi_i^{(m)}$ and $\theta_i^{(f)}$

The mathematical description of every dynamic system can be achieved using a state vector $\mathbf{x} \in \mathbb{R}^{V \times 1}$, input vector

$\mathbf{u} \in \mathbb{R}^{V \times 1}$, and an output vector $\mathbf{y} \in \mathbb{R}^{W \times 1}$. In case, when the time derivative of the state variable vector $\dot{\mathbf{x}} \in \mathbb{R}^{V \times 1}$ and the output vector are not explicit functions of time t, the dynamic system is more generally represented as $\dot{\mathbf{x}} = \mathbf{f}(\mathbf{x}, \mathbf{u})$ and $\mathbf{y} = \mathbf{g}(\mathbf{x}, \mathbf{u})$, where $\mathbf{f}(\cdot) \in \mathbb{R}^{V \times V}$ and $\mathbf{g}(\cdot) \in \mathbb{R}^{W \times V}$ are functionals relating the system state and input to the change in state and output, respectively.

Introducing small perturbations in state vector and input vector and linearizing, we get

$$\begin{aligned} \Delta\dot{\mathbf{x}} &= \mathbf{F}_{\mathrm{S}}\Delta\mathbf{x} + \mathbf{F}_{\mathrm{I}}\Delta\mathbf{u} \\ \Delta\mathbf{y} &= \mathbf{G}_{\mathrm{S}}\Delta\mathbf{x} + \mathbf{G}_{\mathrm{I}}\Delta\mathbf{u} \end{aligned} \tag{2}$$

where $\mathbf{F}_{\mathrm{S}} \in \mathbb{R}^{V \times V}$, $\mathbf{F}_{\mathrm{I}} \in \mathbb{R}^{V \times V}$, $\mathbf{G}_{\mathrm{S}} \in \mathbb{R}^{W \times V}$, and $\mathbf{G}_{\mathrm{I}} \in \mathbb{R}^{W \times V}$ are the system matrix, input matrix, output matrix, and feed-forward matrices, respectively. In order to determine the eigenfrequencies, we solve the characteristic equation:

$$\|\mathbf{F}_{\mathrm{S}} - \lambda\mathbf{I}\| = 0 \tag{3}$$

where $\mathbf{I} \in \mathbb{R}^{V \times V}$ is an identity matrix. Let the eigenvalues of the system be denoted by $\lambda_1, \cdots, \lambda_V$. It is notable that, if (3) is solved for the ith bus, the jth obtained eigenvalue follows the nomenclature λ_{ij}. Next, we define an indicator function $\Im(\mathfrak{Z})$ such that the indicator evaluates to unity when the hypothesis $\mathfrak{Z}$ holds true. Hereafter, we define two hypotheses for the modeling of $\phi_i^{(m)}$ and $\theta_i^{(f)}$, namely Hypotheses 1 and 2, respectively.

$$\begin{aligned} \text{Hypothesis 1}: \mathfrak{Z}_{ij}^{(m)} &\overset{\text{(def)}}{\Longrightarrow} \lambda_m \in (\lambda_{ij} - \Delta\lambda, \lambda_{ij} + \Delta\lambda) \\ \text{Hypothesis 2}: \mathfrak{Z}_{ij}^{(f)} &\overset{\text{(def)}}{\Longrightarrow} f \in (f_{ij} - \Delta f, f_{ij} + \Delta f) \end{aligned} \tag{4}$$

where $f_{ij} = \frac{\Im(\lambda_{ij})}{2\pi}$, $\Delta\lambda$ represents the mode variation, i.e., the proximity to a given mode shape as experienced by a given power system node, and $2(\Delta f)$ is the frequency bandwidth of SSO observed as a virtue of the ijth eigenmode. Therefore, based on the hypotheses, as defined above, we have

$$\begin{aligned} \phi_i^{(m)} &= \Im\left(\mathfrak{Z}_{i1}^{(m)} \vee \mathfrak{Z}_{i2}^{(m)} \vee \cdots \vee \mathfrak{Z}_{iq}^{(m)}\right) \\ \theta_i^{(f)} &= \Im\left(\mathfrak{Z}_{i1}^{(f)} \vee \mathfrak{Z}_{i2}^{(f)} \vee \cdots \vee \mathfrak{Z}_{iq}^{(f)}\right) \end{aligned} \tag{5}$$

where $\vee$ represents the logical OR operation. Thus, $\phi_i^{(m)}$ and $\theta_i^{(f)}$ evaluate to unity if at least one of the involved hypotheses, i.e., $\mathfrak{Z}_{ij}^{(m)}$ and $\mathfrak{Z}_{ij}^{(f)}$, $\forall j = 1, \cdots, q$, respectively, holds true.

The modeling of w_{ij} is presented next.

B. Modeling of Weights w_{ij}

As per definition, w_{ij} represents the importance assigned to the jth eigenvalue of the ith bus. We bifurcate this weight into two disjoint product terms α_i and β_{ij}, such that $w_{ij} = \alpha_i\beta_{ij}$. In this notation, α_i models the ability of a node to contribute to the aggregate SSOs in the grid and β_{ij} captures the contribution of the jth eigenmode of ith node in that aggregate oscillation. Therefore, β_{ij} can be written as

$$\beta_{ij} = \frac{\lambda_{ij}^*}{\sum_{j=1}^{M_i} \|\lambda_{ij}\|} \tag{6}$$

where $(\cdot)^*$ denotes the conjugate operation on a complex number and $\| \cdot \|$ represents the norm operation. Let the

ith node be associated with q features, such that, $\boldsymbol{\varphi}_{i,\Delta t} = \{\varphi_{i,\Delta t}^{(1)}, \varphi_{i,\Delta t}^{(2)}, \cdots, \varphi_{i,\Delta t}^{(q)}\}$, where $\varphi_{i,\Delta t}$ is the feature set observed in the duration Δt. These features are related using the network equations as follows:

$$\begin{aligned} \varphi_{1,\Delta t}^{(1)} &= \psi_i^{(1)}\left(\varphi_{i,\Delta t}^{(1)}, \varphi_{i,\Delta t}^{(2)}, \cdots, \varphi_{i,\Delta t}^{(q)}\right) \\ &\vdots \\ \varphi_{i,\Delta t}^{(q)} &= \psi_i^{(q)}\left(\varphi_{i,\Delta t}^{(1)}, \varphi_{i,\Delta t}^{(2)}, \cdots, \varphi_{i,\Delta t}^{(q)}\right) \end{aligned} \tag{7}$$

where the $\psi(\cdot)$ functions could be modeled through Kirchhoff's voltage/current laws, swing equations, power flow equations, etc. Applying Taylor's expansion in (7) for the modeling of SSOs in the features of $\boldsymbol{\varphi}_{i,\Delta t}$ denoted as $\boldsymbol{\Delta\varphi}_{i,\Delta t}$, we have

$$\begin{aligned} \Delta\varphi_{i,\Delta t}^{(1)} &= \left[\boldsymbol{\Delta\psi}_i^{(1)}\left(\boldsymbol{\varphi}_{i,ss}\right)\right]^T \boldsymbol{\Delta\varphi}_{i,\Delta t} \\ &\vdots \\ \Delta\varphi_{i,\Delta t}^{(q)} &= \left[\boldsymbol{\Delta\psi}_i^{(q)}\left(\boldsymbol{\varphi}_{i,ss}\right)\right]^T \boldsymbol{\Delta\varphi}_{i,\Delta t} \end{aligned} \tag{8}$$

where the subscript ss denotes the set of steady state values, $\Delta(\cdot)$ represents the change in the objective parameter, and T represents the transpose operation. For dimensional compatibility, we must note that $\boldsymbol{\Delta\varphi}_{j,\Delta t}$, $\boldsymbol{\Delta\psi}_i^{(j)}\left(\boldsymbol{\varphi}_{i,ss}\right) \in \mathbb{R}^{q \times 1}$, and their product results in a scalar $\Delta\varphi_{i,\Delta t}^{(j)}$, $\forall j = 1, 2, \cdots, q$. Thus, (8) can be concisely represented as

$$\boldsymbol{\Delta\psi}_i\left(\boldsymbol{\varphi}_{i,ss}\right)\boldsymbol{\Delta\varphi}_{i,\Delta t} = \boldsymbol{\Delta\varphi}_{i,\Delta t} \tag{9}$$

where $\boldsymbol{\Delta\psi}_i\left(\boldsymbol{\varphi}_{i,ss}\right) = [[\boldsymbol{\Delta\psi}_i^{(1)}(\boldsymbol{\varphi}_{i,ss})]^T, \cdots, [\boldsymbol{\Delta\psi}_i^{(q)}(\boldsymbol{\varphi}_{i,ss})]^T]^T \in \mathbb{R}^{q \times q}$. It is noteworthy that, (9) represents an eigenrelation, with a unit magnitude of the corresponding eigenvector. Therefore, to define α_i, we find the contribution of the eigenvector of magnitude 1 amongst a total of q eigenvectors that are obtained for the ith node, i.e., $\alpha_i = \frac{1}{\sum_{j=1}^q \|\lambda_{ij}'\|}$, where λ_{ij}', $\forall j = 1, 2, \cdots, q$ are the eigenvalues of $\boldsymbol{\Delta\psi}_i\left(\boldsymbol{\varphi}_{i,ss}\right)$. The data-based optimization for selection of most qualified nodes is done next.

IV. DATA-BASED OPTIMIZATION FOR DETECTION OF POWER SYSTEM SSO

In this section a PMU data-dependent optimization is proposed for an overall oscillation monitoring in an N-node power network. This serves as a validation for the solution obtained for $(\mathbf{P}1)$. It is worth noting here that, systems fluctuations due to renewable energy sources and (or) other system variables are already recorded in the node datasets. Therefore, the proposed methodology is robust to such fluctuations and can function with similar efficiency in identifying the critical oscillation frequencies of the renewable-integrated systems.

Let $\mu_i \in \{0, 1\}$, $\pi_i \in \{0, 1\}$, and $l_i \in \{0, 1\}$, such that $i \in \mathcal{N}$, be binary decision variables indicating whether a PMU is installed at the ith grid node, whether or not it is chosen for collaboration, and if the PMU is available or lost. The loss of a PMU ($l_i = 0$) could be attributed to a hardware, software, or any network failure, or due to a possible cyber attack. If a PMU is installed at node i, $\mu_i = 1$ and 0 otherwise. Similarly, the value of π_i is decided based on if the PMU at node i is

selected ($\pi_i = 1$) or not selected ($\pi_i = 0$) to be a part of the collaboration for SSO detection. Since optimal placement of PMUs is not in the scope of this research, we assume that there are K optimally placed PMUs, with their locations stored in $\mathbf{L}$, such that $\|\mathbf{L}\|_c = K$. To be able to detect the power system oscillations with least number of PMU involvement, the optimal PMU selection problem is formulated as follows:

$$
\begin{aligned}
(\mathbf{P2}): \quad & \min_{\pi_i} \sum_i l_i \mu_i \pi_i \\
\mathbf{C21}: \quad & \chi_t \geq \chi_0 \\
\mathbf{C22}: \quad & \sum_i l_i \mu_i \pi_i a_i^{(m)} \geq 1, \quad \forall m \\
\mathbf{C23}: \quad & \sum_i l_i \mu_i \pi_i b_i^{(f)} > 1, \quad \forall f \in [0, f_s) \\
\mathbf{C24}: \quad & \sum_i l_i \mu_i \pi_i \leq K \\
\mathbf{C25}: \quad & a_i^{(m)}, b_i^{(f)}, \pi_i, \mu_i, l_i \in \{0,1\}, \quad \forall i, m, f
\end{aligned}
\tag{10}
$$

where $a_i^{(m)}$ is a binary variable that indicates whether the PMU at node i captures measurements from oscillatory mode m. $a_i^{(m)} = 1$ iff PMU i captures measurements from oscillatory mode m, and 0 otherwise. $b_i^{(f)}$ is a binary variable that indicates whether PMU i captures measurements within frequency range f. $b_i^{(f)} = 1$ if the PMU installed at node i captures measurements within frequency range f, and 0 otherwise. Therefore, in case of a PMU loss or compromised PMU operation, a revised PMU selection can be attained by dropping the index of the affected PMU from the set $\mathbf{L}$.

The χ_t-squared test criterion is defined as $\chi_t = \sqrt{\sum_{j=1}^q (\delta\varphi_{\Delta t}^{(j)} \cdot \sigma_{\varphi_{\Delta t}^{(j)}}^{-1})^2}$, where $\delta\varphi_{\Delta t}^{(j)} = \frac{\sum_i \mu_i \pi_i \delta\varphi_{i,\Delta t}^{(j)}}{\sum_i \mu_i \pi_i}$, $\delta\varphi_{i,\Delta t}^{(j)} = \varphi_{i,\Delta t}^{(j)} - \varphi_{i,ss}^{(j)}$, with $\varphi_{i,\Delta t}^{(j)}$ representing the amplitude of jth feature measured by the ith PMU in time window Δt, and q denotes the total features monitored by the PMUs, viz., voltage magnitude, voltage phase, current magnitude, current phase, etc. These features for the ith node are stored in the feature set $\varphi_{i,\Delta t}$ and $\sigma_{\varphi_{\Delta t}^{(j)}}$ represents the standard deviation in the aggregated measurement of the jth feature.

Constraint $\mathbf{C21}$ ensures that the total represented deviation by the chosen PMUs captures a significant proportion of the potential SSOs in the power system. Constraint $\mathbf{C22}$ ensures that the selected PMUs collectively capture measurements from each oscillatory mode in the power system. Constraint $\mathbf{C23}$ focuses on capturing measurements from specific frequency ranges to enable accurate spectral analysis of SSOs. Constraint $\mathbf{C24}$ ensures that the total number of PMUs in collaboration are less than or equal to the maximum PMUs installed in the grid. Finally, the constraint $\mathbf{C25}$ limits $a_i^{(m)}$, $b_i^{(f)}$, and π_i to be a binary constants. The mathematical modeling of $a_i^{(m)}$ and $b_i^{(f)}$ is done next.

A. Mathematical Modeling of $a_i^{(m)}$

Let the ith PMU dataset be denoted as $\mathbf{R}_i \in \mathbb{R}^{p \times q}$, where p is the number of time instances over which the data is recorded. We normalize each column of this dataset by subtracting the respective mean and dividing by the standard deviation of that particular data feature. Let $\tilde{\mathbf{R}}_i$ be the nor-

malized dataset obtained from $\mathbf{R}_i$. We construct a collective data matrix $\mathbf{D}$ of all PMU datasets of size $\mathbb{R}^{p \times (q \times K)}$, such that, $\mathbf{D} = [\tilde{\mathbf{R}}_1, \cdots, \tilde{\mathbf{R}}_K]$. We apply the singular value decomposition (SVD) to obtain $\mathbf{D} = \mathbf{U}\mathbf{\Sigma}\mathbf{V}^T$, where $\mathbf{U} \in \mathbb{R}^{p \times p}$ is an upper triangular matrix, $\mathbf{\Sigma} \in \mathbb{R}^{p \times (q \times K)}$ is the matrix of singular values, $\mathbf{V} \in \mathbb{R}^{(q \times K) \times (q \times K)}$ is a lower triangular matrix, and T represents the transpose operation. Next we define a correlation threshold value τ, such that, $0 \leq \tau \leq 1$, to identify significant correlations between the mode shapes obtained from the theoretical optimization in Section III and the PMU datasets. For the mth oscillatory mode shape, defined by the mth column vector $\mathbf{u}_m \in \mathfrak{C}(\mathbf{U})$ of the matrix $\mathbf{U}$, we calculate the correlation coefficient $\rho(u_m, R_{ij})$ between $\mathbf{u_k}$ and each column of the normalized PMU dataset $\mathbf{R}_i$, where $i \in 1, \cdots, K$, $j \in 1, \cdots, \|\mathfrak{C}(\mathbf{R}_i)\|_c$, and $\mathfrak{C}(\mathbf{R}_i)$ and $\mathfrak{C}(\mathbf{U})$ are the column spaces of matrix $\mathbf{R}_i$ and matrix $\mathbf{U}$, respectively. Mathematically

$$
\rho_{ij}^{(m)} = \rho(u_m, R_{ij}) = \frac{\mathbb{E}[\tilde{\mathbf{u}}_m^T \tilde{\mathbf{R}}_{ij}]}{\sigma_{\mathbf{u}_m} \sigma_{\tilde{\mathbf{R}}_{ij}}}
\tag{11}
$$

where $\tilde{\mathbf{u}}_m = \mathbf{u}_m - \mu_{\mathbf{u}_m} \mathbf{f}_{p \times 1}$, $\mu_{\mathbf{u}_m} = \mathbb{E}[\mathbf{u}_m]$, with $\mathbf{f}_{p \times 1}$ being a vector of ones of size $p \times 1$, and $\sigma_{\mathbf{u}_m} = \mathbb{E}\left[(\mathbf{u}_m - \mu_{\mathbf{u}_m})^T (\mathbf{u}_m - \mu_{\mathbf{u}_m})\right]$. Thus, for the indicator function $\Im(\cdot)$, introduced in the explanatory notes after (3), we define the hypothesis as follows, Hypothesis 3: $\mathfrak{Z} \overset{(\text{def})}{\Longrightarrow} \rho_{ij}^{(m)} \geq \tau$. Therefore, $a_i^{(m)}$ is defined as

$$
a_i^{(m)} = \Im\left(\left\{\rho_{i1}^{(m)} \geq \tau\right\} \vee \left\{\rho_{i2}^{(m)} \geq \tau\right\} \vee \cdots \vee \left\{\rho_{iq}^{(m)} \geq \tau\right\}\right).
$$

It is notable that, $a_i^{(m)}$ evaluates to 1 if the mth oscillatory mode posses high correlation with at least one feature of the measurements collected by the ith PMU, i.e., with one column of the data matrix $\mathbf{R}_i$.

B. Mathematical Modeling of $b_i^{(f)}$

From the state-space model of the system deduced in (2) and the corresponding eigenvalues obtained through (3), the frequency (should not be confused with the nominal frequency of the grid, i.e., 50 or 60 Hz) components of significance are given by the imaginary part of the eigenvalues, i.e., the rth eigenfrequency component is written as $f_r = \frac{\Im(\lambda_r)}{2\pi}$, such that $\mathbf{f} = [f_1, \cdots, f_V]^T \in \mathbb{R}^{V \times 1}$ is a vector of eigenfrequencies, where $\Im(\cdot)$ denotes the imaginary part operation. Next, we take the row-wise Fourier transform of the ith PMU dataset. Mathematically

$$
\mathfrak{R}_{ij} = \mathcal{F}\left(\tilde{\mathbf{R}}_{ij}\right), \quad \text{where } \tilde{\mathbf{R}}_{ij} \in \mathfrak{C}\left(\tilde{\mathbf{R}}_{ij}\right)
\tag{12}
$$

where $\mathcal{F}(\cdot)$ represents the Fourier transform operation. The power spectral density (PSD) $\mathfrak{P}_{ij}$ is represented as

$$
\mathfrak{P}_{ij} = \mathfrak{K}(\mathfrak{R}_{ij})\left(\|\mathfrak{K}(\mathfrak{R}_{ij})\|_c\right)^{-1}
\tag{13}
$$

where $\mathfrak{K}(\cdot)$ represents an element-wise norm-squared operation on the vector $\mathfrak{R}_{ij}$. We define the frequency component f from the $\mathfrak{P}_{ij}$ as $\mathfrak{P}_{ij}^{(f)}$ and define a new hypothesis as follows, Hypothesis 4: $\mathfrak{Z} \overset{(\text{def})}{\Longrightarrow} \mathfrak{P}_{ij}^{(f)} \geq \mathfrak{P}_{\text{th}}$. Therefore, $b_i^{(f)}$ is defined

as

$$b_i^{(f)} = \Im\left(\left\{\mathfrak{P}_{i1}^{(f)} \geq \mathfrak{P}_{\text{th}}\right\} \vee \left\{\mathfrak{P}_{i2}^{(f)} \geq \mathfrak{P}_{\text{th}}\right\} \vee \cdots \vee \left\{\mathfrak{P}_{iq}^{(f)} \geq \mathfrak{P}_{\text{th}}\right\}\right).$$

It is worth observing that, $b_i^{(f)}$ evaluates to 1 if the frequency component f is dominant in the PSD of at least one data feature monitored by the ith PMU. The optimization problems ($\mathbf{P}$1) and ($\mathbf{P}$2) are solved using the *intlinprog* function of MATLAB. In the next subsection, we relax the noiseless (ideal) assumption on the measurements noted by the PMU data, and re-evaluate the parameters involved in the optimization formulated in (10). As a result, the related hypotheses are restructured to impart immunity against the measurement noise suffered by the PMU data to the data-based optimization.

C. Impact of Measurement Noise

If the attribute set measured by the PMU is denoted as $\mathcal{A}$, the measurement noise-infested dataset can be represented as $\hat{\mathbf{R}}_i(\mathcal{A}) = \mathbf{R}_i(\mathcal{A} + \delta\mathcal{A})$, where $\delta\mathcal{A}$ is the deviation in the measurements of the attributes. For relative small error values, which is mostly the case in well-maintained IoT units, linearizing using the Taylor's expansion returns

$$\hat{\mathbf{R}}_i(\mathcal{A} + \delta\mathcal{A}) = \mathbf{R}_i(\mathcal{A}) + \delta\mathcal{A}\frac{\partial\mathbf{R}_i(\mathcal{A})}{\partial\mathcal{A}}. \quad (14)$$

Here onwards, for brevity, we drop the arguments and represent $\delta\mathcal{A}\frac{\partial\mathbf{R}_i(\mathcal{A})}{\partial\mathcal{A}} = \mathbf{E}_i$, which is termed as the measurement error, such that $\hat{\mathbf{R}}_i = \mathbf{R}_i + \mathbf{E}_i$. Let $\mathbf{E}_i \in \mathbb{R}^{p\times q}$ denote the noise matrix corresponding to the PMU measurements in $\mathbf{R}_i \in \mathbb{R}^{p\times q}$, such that the columns of $\mathbf{E}_i$ denote the noise in different attributes measured by the PMU and the rows describe the time-evolution of the noise. Then, as established in literature, it is fair to assume that the noise follows a zero-mean Gaussian distribution profile [36]. Therefore, based on a matrix noise structure, $\mathbf{E}_i$ follows a matrix normal distribution $\mathcal{MN}_{p,q}(\mathbf{0}, \mathbf{L}, \mathbf{M})$, given by

$$p(\mathbf{E}_i|\mathbf{0}, \mathbf{L}, \mathbf{M}) = \frac{\exp\left(-\frac{1}{2}\text{Tr}\left[\mathbf{M}^{-1}\mathbf{E}_i^T\mathbf{L}^{-1}\mathbf{E}_i\right]\right)}{(2\pi)^{pq/2}|\mathbf{M}|^{p/2}|\mathbf{L}|^{q/2}} \quad (15)$$

where $\text{Tr}(\cdot)$ is the trace operation, $\mathbb{E}[\mathbf{E}_i] = \mathbf{0}$, and $\mathbb{E}[\mathbf{E}_i\mathbf{E}_i^T] = \mathbf{L}\,\text{Tr}(\mathbf{M})$. Therefore, the revised collective data matrix $\hat{\mathbf{D}}$ of all PMU datasets, is given by $\hat{\mathbf{D}} = \mathbf{D} + \mathbf{E}$, where $\mathbf{E} = [\mathbf{E}_1, \cdots, \mathbf{E}_K]$. Again, using SVD, we write

$$\hat{\mathbf{D}} = \hat{\mathbf{U}}\hat{\mathbf{\Sigma}}\hat{\mathbf{V}}^T \quad (16)$$

where $\hat{\mathbf{U}}$ is the revised upper triangular matrix, $\hat{\mathbf{\Sigma}}$ is the matrix of revised singular values, and $\hat{\mathbf{V}}$ is the revised lower triangular matrix for the error-prone PMU data measurements.

Lemma 1. *For any non-Hermitian perturbed matrix $\hat{\mathbf{D}}$, related to its unperturbed counterpart $\mathbf{D}$ as, $\hat{\mathbf{D}} = \mathbf{D} + \mathbf{E}$, its SVD can be expressed as*

$$\hat{\mathbf{D}} = \mathbf{PU}(\mathbf{\Sigma} + \mathbf{\Delta})\mathbf{V}^T\left[2\mathbf{I} - (\mathbf{D}^T\mathbf{D})^{-1}\mathbf{D}^T\mathbf{PD}\right]$$

where $\hat{\mathbf{\Sigma}} = \mathbf{\Sigma} + \mathbf{\Delta}$, such that the ith singular value obtained for the true and perturbed matrices follow, $|\mathbf{\Delta}_i| = |\sigma_i - \hat{\sigma}_i| \leq \|\mathbf{E}\|_F$, $\forall i$, with $\mathbf{\Delta}_i$ being the ith value of $\mathbf{\Delta}$ matrix, σ_i and $\hat{\sigma}_i$ denoting the singular values for true and perturbed

matrices, respectively, and $\|\cdot\|_F$ represents the Forbenius norm of the involved matrix. $\hat{\mathbf{U}} = \mathbf{PU}$ represents the rotational relationship between left eigenspaces of the unperturbed and perturbed matrices, such that

$$(\mathbf{M}^T\mathbf{M})^{-1}\mathbf{M}^T\mathbf{PM} - (\mathbf{D}^T\mathbf{D})^{-1}\mathbf{D}^T\mathbf{PD} = (\mathbf{M}^T\mathbf{M})^{-1}\mathbf{M}^T\mathbf{E} - \mathbf{I}$$

where $\mathbf{M} = \mathbf{U}\mathbf{\Delta}\mathbf{V}^T$, $\mathbf{D} = \mathbf{U}\mathbf{\Sigma}\mathbf{V}^T$, and $\mathbf{I}$ represents the identity matrix.

Proof. See Appendix A. $\square$

The above Lemma provides an interesting insight into the relation between the SVD of noisy and noise-free versions of a matrix. For a non-Hermitian matrix, the SVD of the noisy matrix can be represented solely in terms of the rotation of one of the eigenspaces. First, we establish the signal-to-noise power ratio (SNPR) to quantify the noise-level present in the PMU measurements. SNPR is defined as follows

$$\text{SNPR (dB)} = 10\log_{10}\frac{P_{\text{S}}}{P_{\text{N}}}\text{(dB)} \quad (17)$$

where P_{N} and P_{S} are the noise power and signal power, respectively. Mathematically, the power of a matrix $\boldsymbol{\chi}$ with T time samples and A attributes, is defined as follows

$$P_{\mathcal{M}} = \frac{1}{AT}\sum_{j=1}^{A}\mathcal{F}(\boldsymbol{\chi}_j)^T\mathcal{F}(\boldsymbol{\chi}_j) \quad (18)$$

where $\boldsymbol{\chi}_j$ represents the jth column of matrix $\boldsymbol{\chi}$ and $\mathcal{M} = \{N, S\}$. Next, we analyze the impact of measurement noise $\mathbf{E}$ on the correlation computed in (11).

Lemma 2. *The Pearson's correlation computed from the perturbed SVD is given as $\hat{\rho}_{ij}^{(m)} = \rho_{ij}^{(m)}\left(\frac{1-\zeta_1}{1+\zeta_2}\right)$, where $\rho_{ij}^{(m)}$ is the correlation computed from the error-free SVD decomposition, $\zeta_1 = \frac{(\mathbf{DD}^T)^{-1}\mathbf{DQ}_0}{\mathbb{E}[\tilde{\mathbf{u}}_m^T\tilde{\mathbf{R}}_{ij}]}$, and $\zeta_2 = \frac{\mathbf{u}_m^T(\mathbf{DD}^T)^{-1}\mathbf{DQ}_1\mathbf{D}^T(\mathbf{DD}^T)^{-1}\mathbf{u}_m}{2\sigma_{\tilde{\mathbf{u}}_m}^2} + \frac{\mathbb{E}[\mathbf{E}_{ij}^T\mathbf{E}_{ij}]}{2\sigma_{\tilde{\mathbf{R}}_{ij}}^2}$.*

Proof. See Appendix B. $\square$

Therefore, from Lemma 2, we note that if we revise the threshold as $\tau \to \tau\left(\frac{1-\zeta_1}{1+\zeta_2}\right)$, the decision rule for $a_i^{(m)}$ does not vary between the measurement noise-infested and noise-free PMU data. Next, we remodel $b_i^{(f)}$ to address the measurement noise $\mathbf{E}$.

Lemma 3. *The revised value of $b_i^{(f)}$ can be restored to its original value by changing the threshold for the fourth hypothesis as, $\mathfrak{P}_{\text{th}} \to \mathfrak{P}_{\text{th}} + \frac{\mathfrak{K}(\partial\mathfrak{R}_{ij})}{\|\mathfrak{K}(\mathfrak{R}_{ij})\|_c}$, where $\partial\mathfrak{R}_{ij}$ is the Fourier spectrum of the measurement error in the PMU data.*

Proof. See Appendix C. $\square$

Next, we show the results obtained from the optimization formulations ($\mathbf{P}$1) and ($\mathbf{P}$2) with the adversities considered in Section II in proving the applicability of the proposed approach in detecting the SSOs in the power network.

V. RESULTS AND DISCUSSIONS

This section presents the results for the optimization problems ($\mathbf{P}$1) and ($\mathbf{P}$2), wherein we simulate the standard IEEE

TABLE II: Multi-machine system configuration for the IEEE 5-bus (3-machine) test system in Fig. 2 [37]

Machine	Parameters		
	Machine rating	Exciter-stabilizer	Turbine-governor
Machine 1	Rating: 555 MVA, 24 kV In p.u. based on machine rating: $X_{ad} = 1.138$, $X_f = 0.0781$, $X_{rd} = 0.088$ $X_{aq} = 1.038$, $X_{Kq} = 0.227$, $r_a = 0.00153$ $r_f = 0.000748$, $r_{Kd} = 0.00805$, $r_{Kq} = 0.00253$ $H = 3.38$ sec, $P_G = 0.9$, $\Omega_G = 0.44$	$K_e = 350$, $K_Q = 6$, $\tau_v = 0.03$, $\tau_e = 0.002$ $\tau_Q = 1.4$, $\tau_a = 0.121$, $\tau_x = 0.033$ sec	$K_g = 0.04$, $\tau_3 = 0.1$, $\tau_4 = 0.3$ sec
Machine 2	Rating: 635 MVA, 24 kV In pu based on machine rating: $X_{ad} = 0.945$, $X_f = 0.0755$, $X_{Kd} = 0.085$ $X_{aq} = 0.945$, $X_{Kq} = 0.085$, $r_a = 0.00153$ $r_f = 0.00039$, $r_{Kd} = 0.00805$, $r_{Kq} = 0.00253$ $H = 5.4$	$K_e = 200$, $K_Q = 10$, $\tau_v = 0.03$, $\tau_e = 0.002$ $\tau_Q = 1.4$, $\tau_a = 0.12$, $\tau_x = 0.033$ sec	$K_g = 0.04$, $\tau_3 = 0.1$, $\tau_4 = 0.3$ sec
Machine 3	Rating: 66 MVA, 13.8 kV In pu based on machine rating: $X_{ad} = 0.567$, $X_f = 0.14$, $X_{rd} = 0.087$ $X_{aq} = 0.33$, $X_{Kq} = 0.163$, $r_a = 0.002$ $r_f = 0.00035$, $r_{rd} = 0.02$, $r_{rq} = 0.04$ $H = 4.29$ sec, $P_G = 0.2$, $Q_G = 0.7$	$K_A = 200$, $K_E = -0.17$, $K_F = 0.04$, $S_E = 0.95$ $\tau_A = 0.05$, $\tau_E = 0.95$, $\tau_F = 1$, $\tau_v = 0.03$ sec	$K_g = 0.04$, $\tau_1 = 0.4$, $\tau_3 = 0.4$, $\tau_5 = 0.35$ sec
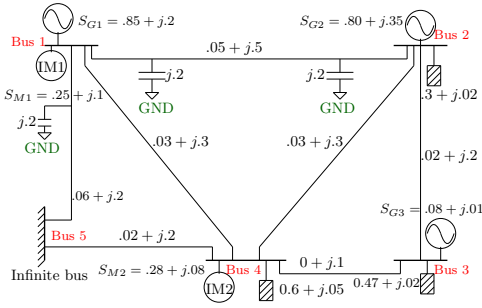
Fig. 2: Network diagram of IEEE 5-bus (3 machine) test system.

TABLE III: IEEE 5-bus test system's eigenvalues at base condition

Bus 1	Bus 2	Bus 3	Bus 4	Bus 5
$-.542 \pm j1.854$	-2.823	-10.42	$-19.96 \pm j376.2$	-49.95
$-.628 \pm j5.943$	$-2.975 \pm j9.947$	-10.46	-20.58	-52.21
$-.691 \pm j.121$	-3.195	-13.21	-30.54	-152.6
$-.750$	$-3.218 \pm j2.004$	$-13.06 \pm j18.13$	-30.92	-167.8
-1	$-7.576 \pm j20.96$	-13.58	-33.02	$-239.5 \pm j1365$
-1.334	$-8.312 \pm j21.23$	$-14.41 \pm j376.5$	-34.01	-500.6
$-1.436 \pm j6.242$	$-8.555 \pm j27.10$	$-15.17 \pm j430.3$	$-34.39 \pm j560.9$	-502.1

test systems and collect PMU data generated by the industrially accepted RSCAD simulation platform. The results are validated for IEEE 5, 14, 30, 39, 57, and 118-bus systems. In our analysis, we have considered a total of K oscillation modes, where

$$K = N_T - N_{PV} - 1 + M + A \qquad (19)$$

where N_T denotes the total buses in the system, N_{PV} denotes the total number of PV (or generator) buses, M denotes the total number of machines, and A are the additional system states arising from other dynamic components. The results presented in Tables III through VII consider $A = 0$ for tractability of analysis. In the results that follow, we set the χ-squared test energy threshold χ_0 as 0.95. This threshold can be set between 0 and 1, based on the amount of total disturbance energy that requires to be captured for gathering significant information on the disturbance signature in the power network.

A. Example: IEEE 5 Bus (3-Machine) Test System

Fig. 2 depicts the structure and operating conditions of IEEE 5-bus (3-machine) system, with its system parameters defined

in Table II. To consider the aspect of additional system states, in this subsection, we provide a detailed analysis on the use of our proposed oscillation identification methodology considering a total of 35 oscillation modes (c.f. Table III). Buses 1, 2, and 3 consists of fossil fuel-based, nuclear power-based, and smaller hydro power-based generating units. Machines 1 and 2 have static exciters and stabilizing signals fed-back depending on the rotor speed of the respective machines. Machine 3 has a type 1 exciter, with governor effects included in the simulation of all the three machines. System loads are represented as linear static elements located at buses 2, 3, and 4. Further, two dynamic equivalent models for induction motor loads are envisaged at buses 1 and 4. All per unit values mentioned in Fig. 2 are calculated as per the base values of 600 MVA and 24 kV. Based on above system description, the detailed state update equations for each bus is derived as detailed in [37] and the corresponding eigenvalues are mentioned in Table III.

For the sake of covering all important eigenfrequency ranges, we choose the frequency ranges of importance as 0-1 Hz, 1-5 Hz, 50-80 Hz, and 190-220 Hz, with Δf for these ranges defined as half of the frequency range. For example, for the range 0-1 Hz, the central frequency is 0.5 Hz, with $\Delta f = 0.5$, i.e., the frequency bandwidth of SSO. Therefore, using Table III, we get $\theta_1^{(f)} = 1$ for $f = 0.5$ Hz, while $\theta_i^{(f)} = 0$, $\forall i = 2, \cdots, 5$. Next, we define the mode range of importance starting from 0-5 in steps of 5 and $\Delta \lambda = 2.5$, i.e., 0-10, 10-20, and so on. The central mode value is naturally the mid-point of the mode range. Thus, $\phi_1^{(m)} = \phi_2^{(m)} = 1$ for $m = 5$, while $\phi_1^{(m)} = 0$, $\forall i = 3, 4, 5$. Similarly, all other ϕs and θs can be computed for the optimization problem (**P**1).

On solving (**P**1), we obtain the optimal solution as 2, 5. Further, on solving (**P**2) using the PMU data generated using RSCAD, we obtain the same solution vector, i.e., 2, 5. This verifies the theoretical results obtained for (**P**1) through the solution obtained for (**P**2) using the simulated PMU dataset.

Remark 2. *It is notable that, since the optimization problem in (**P**1) and (**P**2) already obtain the most qualified nodes as per the frequency and mode ranges, the obtained solution helps in capturing the information about the disturbances/SSOs in the entire network in a least-time and tap manner, i.e., by*

TABLE IV: Optimal solution of the most qualified PMU selection for standard IEEE test systems for capturing all eigenfrequencies under normal grid conditions; Prop.: proposed, Conv.: conventional

IEEE test system	Strategic PMU placement [38]	PMU data-based optimization	Theoretical optimization	Execution time (sec)		% red. in req. nodes	% energy captured
				Prop.	Conv. [33]		
14-bus	2, 6, 7, 9	2, 7	2, 7	1.013	8.74	50	99.57
30-bus	1, 7, 8, 10, 11, 12, 18, 23, 26, 30	7, 11, 18, 26	7, 11, 18, 26	1.793	23.44	60	99.52
39-bus	2, 6, 9, 12, 14, 17, 22, 23, 29, 32, 33, 34, 37	6, 12, 22, 29, 33, 37	6, 12, 22, 29, 33, 37	1.996	28.73	53.85	99.47
57-bus	2, 6, 10, 12, 19, 22, 25, 27, 32, 36, 38, 41, 45, 46, 49, 52, 55, 57	2, 6, 10, 22, 27, 32, 38, 57	2, 6, 10, 22, 27, 32, 38, 57	2.017	40.03	55.56	99.32
118-bus	2, 5, 10, 12, 15, 17, 21, 25, 29, 34, 37, 41, 45, 49, 53, 56, 62, 64, 72, 73, 75, 77, 80, 85, 87, 91, 94, 101, 105, 110, 114, 116	2, 10, 15, 21, 29, 34, 41, 53, 56, 62, 72, 73, 75, 80, 87, 91, 94, 105, 110, 116	2, 10, 15, 21, 29, 34, 41, 53, 56, 62, 72, 73, 75, 80, 87, 91, 94, 105, 110, 116	4.113	100.75	37.50	99.34
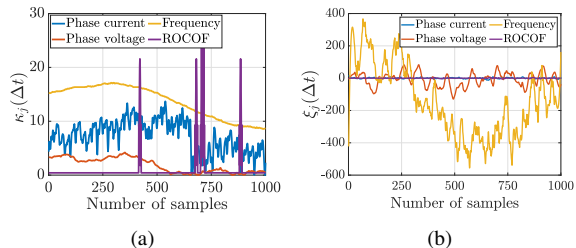
Fig. 3: (a) Time variation of the jth grid feature and (b) variation of chi-squared metric with the change in the value of jth grid feature.

tapping/analyzing least nodes/buses of the network.

B. Characterization of Critical Grid Feature

From the joint analysis of the PMU dataset obtained through the RSCAD simulation, we plot the variation of $\kappa_j(\Delta t) = \frac{\delta \varphi_{\Delta t}^{(j)}}{\sigma_{\varphi_{\Delta t}}^{(j)}}$ and $\xi_j(\Delta t) = \lim_{\Delta t \to 0} \frac{d\chi_t}{d\alpha_j(\Delta t)}$ with the number of samples, denoting the time variation of the jth grid feature from the grid feature set and the variation of the chi-squared disturbance metric with the change in the value of jth grid feature. κ_j and ξ_j metrics define the time sensitivity of the jth parameter and the sensitivity of chi-squared metric with the jth parameter value. From Fig. 3(a), we note that frequency and ROCOF features demonstrate highest variability with time. Therefore, these features are most important in determining the presence of disturbance in the power grid network. From Fig. 3(b), we observe that, change in frequency and voltage-phase causes maximum impact to the chi-squared disturbance metric. In conclusion, frequency and voltage-phase are most critical in identifying disturbance in a grid. It is notable that, this inference is consistent with the well known 'swing equation'.

C. Optimal Solution to Qualified Node Selection

Table IV presents the solution to the 'qualified node selection' optimization problem. The results from the theoretical optimization in ($\mathbf{P}$1) are mentioned in the second column, which are verified by solving ($\mathbf{P}$2) for $l_i = 1 \ \forall i$, i.e., perfect (not compromised) PMU operation scenario, using the simulated PMU data gathered from RSCAD. The solution to ($\mathbf{P}$2) is tabulated in the third column. First, we note that the results obtained from the theoretical optimization, i.e., ($\mathbf{P}$1), match the results obtained from the data-based optimization, i.e., ($\mathbf{P}$2). Next, it can be observed that, by the virtue of selecting the most qualified nodes, the time required in identifying the disturbances/SSOs in the power network reduces significantly.

The final column shows the amount of energy from the power network disturbances that is captured using the data from the selected qualified nodes. This is computed as the ratio of the total energy captured by joint analysis of the most qualified nodes obtained through optimizing ($\mathbf{P}$1) and ($\mathbf{P}$2) to the total energy of the disturbances present in the network. It was noted that the captured disturbance energy is close to $> 99\%$. Therefore, we conclude that, by choosing the most qualified nodes for identifying the disturbances in the power network, it is ensured that the disturbances at the critical frequencies, i.e., the eigenfrequencies, are noted with certainty, resulting in a robust network protection and control. We further draw attention towards the reduction in the number of nodes required to be co-analyzed for the identification of disturbances. For example, for the IEEE 57-bus system, the number of required nodes is reduced by $\approx 60\%$, leading to a $\approx 96\%$ faster analysis time. A careful observation reveals that the number of required nodes, considering all test systems, reduces by a minimum of 50%, leading to communication and analysis of a reduced data footprint.

Here, we verified the validity of the data-based optimization formulation by demonstrating its correspondence with the proposed theoretical optimization in ($\mathbf{P}$1). Therefore, here onwards, we only focus on the solution to the data-based optimization in ($\mathbf{P}$2) under various adversities.

Remark 3. *It is noteworthy that, the reduction in the number of nodes to be co-analyzed for identifying the disturbances in the power network, depends on the grid incidence matrix, i.e., the connection between the nodes. In essence, if the network graph is highly connected, co-analysis of a lesser number of nodes could lead to a sufficient detection for capturing a significant fraction of energy in the disturbance wave.*

D. Qualified Node Selection Under Grid Adversities

This subsection discusses the solution to the most qualified node selection optimization while considering single PMU loss and single line loss conditions. We simulate PMU loss with $l_i = 0$, for the lost PMU and the single line loss situation by changing the grid incidence matrix, which directly impacts (2) through (9). Further, for a fair analysis under such considerations, we start by utilizing the optimization suggested in [38], which considers providing in-advance redundancy for such grid adversities. Next, for investigating into the most critical situations, we consider the loss of PMU which is placed at the node with highest incidence and the loss of power line that leads to the loss in connection between high incidence nodes or the nodes connecting the buses with generating units. From Table V, we observe that, under single PMU loss, the choice of the most qualified nodes changes for all the IEEE bus systems. However, the selected PMUs can

TABLE V: Optimal solution for the selection of the most qualified PMUs for capturing all eigenfrequencies considering single PMU loss in perturbed standard IEEE test systems; Prop.: proposed, Conv.: conventional

IEEE test system	Single PMU loss		Execution time (sec)		% red. in req. nodes	% energy captured
	Strategic PMU placement [38]	PMU data-based optimization	Prop.	Conv. [33]		
14-bus	1, 2, 3, 4, 5, 6, 9, 10, 11, 12, 13, 14	2, 9, 14	1.519	26.649	61.54	99.03
30-bus	1, 2, 3, 4, 7, 10, 12, 13, 14, 15, 16, 17, 18, 19, 20, 23, 24, 28, 29, 30	2, 18, 23, 28, 29	2.241	48.536	66.67	99.13
39-bus	14, 15, 19, 20, 23, 24, 25, 26, 27, 28, 29, 30, 31, 32, 33, 34, 35, 36, 37, 38, 39	14, 19, 27, 28, 30, 38, 39	2.472	46.834	51.85	99.15
57-bus	2, 3, 8, 9, 10, 12, 16, 17, 18, 19, 20, 23, 28, 29, 30, 31, 32, 33, 38, 41, 43, 45, 48, 49, 51, 52, 53, 54, 55, 56, 57	2, 17, 20, 23, 28, 30, 32, 38, 45, 57	2.902	70.075	59.52	99.22
118-bus	1, 2, 6, 7, 11, 12, 13, 14, 15, 16, 17, 19, 21, 22, 23, 24, 25, 27, 29, 32, 36, 41, 42, 43, 44, 46, 47, 48, 49, 50, 51, 52, 53, 55, 56, 57, 58, 60, 62, 65, 66, 67, 68, 69, 72, 73, 74, 75, 76, 77, 78, 79, 80, 81, 83, 85, 86, 87, 88, 89, 90, 92, 94, 95, 97, 98, 99, 100, 101, 102, 103, 104, 106, 106, 107, 108, 109, 110, 110, 111, 112, 113, 113, 114, 115, 116, 117, 118	1, 11, 17, 21, 27, 46, 49, 52, 55, 57, 60, 67, 72, 74, 78, 80, 86, 88, 92, 101, 103, 110, 116	4.652	277.803	62.39	99.25

TABLE VI: Optimal solution of the most qualified PMU selection for standard IEEE test systems for capturing all eigenfrequencies under line loss; Prop.: proposed, Conv.: conventional

IEEE test system	Single line loss		Execution time (sec)		% red. in req. nodes	% energy captured
	Strategic PMU placement [38]	PMU data-based optimization	Prop.	Conv. [33]		
14-bus	1, 2, 4, 6, 8, 9, 11, 13	2, 9, 13	2.375	34.892	37.50	99.13
30-bus	1, 3, 5, 7, 8, 10, 11, 12, 15, 17, 19, 20, 22, 24, 26, 28, 29, 30	8, 11, 19, 26, 29	4.105	59.372	44.44	99.20
39-bus	1, 2, 3, 6, 8, 9, 11, 13, 14, 16, 17, 19, 22, 23, 26, 29, 32, 34, 37	1, 6, 13, 23, 26, 34, 37	5.107	59.823	31.58	99.22
57-bus	1, 2, 4, 6, 9, 12, 15, 19, 20, 22, 24, 26, 28, 29, 30, 31, 32, 35, 36, 38, 39, 41, 43, 45, 46, 47, 50, 51, 53, 54, 56, 57	1, 6, 9, 19, 22, 28, 32, 39, 46, 53	7.032	86.728	46.88	99.27
118-bus	1, 2, 5, 7, 9, 10, 11, 12, 15, 17, 19, 21, 22, 25, 26, 28, 29, 34, 35, 37, 40, 41, 43, 45, 46, 49, 50, 52, 53, 56, 58, 59, 62, 63, 65, 67, 68, 70, 71, 72, 75, 76, 77, 79, 80, 84, 85, 87, 89, 91, 92, 94, 96, 100, 101, 105, 107, 109, 110, 113, 114, 115	5, 9, 15, 21, 28, 34, 40, 50, 52, 56, 62, 72, 76, 79, 84, 87, 89, 91, 94, 101, 105, 109, 115	9.127	330.795	46.67	99.29

still capture $> 99\%$ of the energy in the disturbance wave, which is computed as detailed in the previous subsection. Furthermore, since the proposed optimization finds an optimal PMU group, which is significantly lesser than the total PMUs deployed in the network, the time required to detect the network oscillations reduces significantly, such as 94.23%, 95.38%, 94.72%, 95.86%, and 98.33% for IEEE 14, 30, 39, 57, and 118-bus system, respectively.

The optimization solution with single line loss in presented in Table VI. Again, we note that the optimal PMU set changes when a physical loss of line is considered. However, since the optimization ensures a particular fraction of the disturbance energy getting captured, sufficient monitoring of power network SSOs is always ensured. Notably, the execution time to identify the SSOs increases under line loss as compared to PMU loss, which is the result of more PMU data that has to be analyzed in such conditions. It is notable that, under any adversity, the increase in execution time in the proposed SSO identification framework, involving the co-analysis of data from multiple PMUs is minimal. In contrast, the execution time with the conventional strategy varies significantly (on an average 20%) under line loss conditions. This is by the virtue of a decorrelation introduced in the PMU data arising from the loss of physical connection in the network graph. *In summary, we note that the proposed optimization significantly reduces the processing ($\approx 95\%$) time while still detecting a significant fraction of SSO energy ($\approx 99\%$) with a data footprint reduction of 75%, considering all test systems, under single PMU as well as single line loss conditions.*

E. Qualified Node Selection in Presence of PMU Impairments

Earlier, we discussed the affect of grid adversities on the solution to the optimal selection of most qualified PMUs for detecting power network SSOs. However, it is important to realize that there is another class of adversities that results from a measurement noise-infested real-field data or a compromised PMU operation arising from data breach and (or) malicious attack on the PMU. In such cases, it is important for the proposed optimization framework to find a revised optimal set of PMUs for detecting the network oscillations. Since identifying such adversities are beyond the scope of this research, we assume that such events are detected using the strategy proposed in [35]. From Table VII we note that, as the data becomes infested with more measurement noise, i.e., a lower SNPR, the optimal PMU selection changes considerably, with more number of PMUs (than in the normal operating conditions) being chosen for best results. Naturally, if the optimization results in choosing all the PMUs placed in the network, the fraction of disturbance energy that can be captured reduces. However, since the proposed optimization utilizes a collective analysis of multiple PMU datasets, the reduction in the fraction of disturbance energy that was captured is not significant. It is particularly noteworthy that, for larger SNPR values, i.e., SNPR ≥ 0 dB, the revision in the values of $a_i^{(\mathrm{m})}$ and $b_i^{(\mathrm{f})}$ suggested through Lemma 2 and Lemma 3, respectively, helps to maintain the same optimal PMU set while capturing $> 99\%$ of the disturbance energy.

Next, Table VIII presents the solution to the most qualified node selection optimization, considering compromised PMU operation. In the analysis, we assume that, the PMU placed at the bus with highest order of incidence is compromised (represented using the numbers in bracket in Table VIII for each IEEE test system). It is observed that, with compromised PMU operation, a higher number of PMUs are selected in the process of optimization for detecting the critical frequencies present in the power network disturbance, while still capturing $> 99\%$ of the energy in the disturbance wave. Further, it can be noted that the execution time for detecting $> 99\%$ of the energy in disturbance wave increases in case of the

TABLE VII: Optimal solution of the most qualified PMU selection using measurement noise-infested PMU data for standard IEEE test systems for capturing all eigenfrequencies under normal grid conditions

IEEE test system	SNPR= −10 dB		SNPR= 0 dB		SNPR= 10 dB	
	PMU data-based optimization	% energy captured	PMU data-based optimization	% energy captured	PMU data-based optimization	% energy captured
14-bus	$2, 6, 7, 9$	95.61	$2, 7$	99.56	$2, 7$	99.56
30-bus	$1, 7, 8, 10, 18, 23, 26, 30$	97.08	$7, 11, 18, 26$	99.52	$7, 11, 18, 26$	99.52
39-bus	$2, 9, 12, 14, 23, 29, 32, 34, 37$	98.79	$6, 12, 22, 29, 33, 37$	99.44	$6, 12, 22, 29, 33, 37$	99.44
57-bus	$10, 12, 19, 25, 27, 36, 41, 46, 52,$ $55, 57$	99.28	$2, 6, 10, 22, 27, 32, 38, 57$	99.30	$2, 6, 10, 22, 27, 32, 38, 57$	99.31
118-bus	$5, 12, 17, 21, 25, 29, 37, 41, 45, 49, 56, 64,$ $72, 75, 77, 80, 85, 87, 91, 94, 101, 110, 116$	99.32	$2, 10, 15, 21, 29, 34, 41, 53, 56, 62, 72,$ $73, 75, 80, 87, 91, 94, 105, 110, 116$	99.33	$2, 10, 15, 21, 29, 34, 41, 53, 56, 62, 72,$ $73, 75, 80, 87, 91, 94, 105, 110, 116$	99.33

TABLE VIII: Optimal solution of the most qualified PMU selection using measurement noise-infested PMU data for standard IEEE test systems for capturing all eigenfrequencies under compromised PMU operation

IEEE test system	Normal PMU operation (SNPR = 10 dB)			Compromised PMU operation at highest incidence node (SNPR = 10 dB)		
	PMU data-based optimization	% energy captured	Execution time (sec)	PMU data-based optimization	% energy captured	Execution time (sec)
14-bus	$2, 7$	99.56	1.013	$6, 7, 9 \ (2)$	99.51	1.597
30-bus	$7, 11, 18, 26$	99.52	1.793	$8, 10, 18, 26, 30 \ (7)$	99.43	2.359
39-bus	$6, 12, 22, 29, 33, 37$	99.44	1.996	$2, 9, 14, 22, 23, 32, 34 \ (33)$	99.41	3.57
57-bus	$2, 6, 10, 22, 27, 32, 38, 57$	99.31	2.017	$2, 12, 25, 27, 32, 41, 46, 52, 57 \ (38)$	99.22	4.402
118-bus	$2, 10, 15, 21, 29, 34, 41, 53, 56, 62, 72,$ $73, 75, 80, 87, 91, 94, 105, 110, 116$	99.33	4.113	$5, 12, 15, 21, 29, 37, 45, 53, 56, 62, 64, 72, 73,$ $75, 77, 87, 91, 94, 101, 105, 110, 116 \ (80)$	99.30	6.464
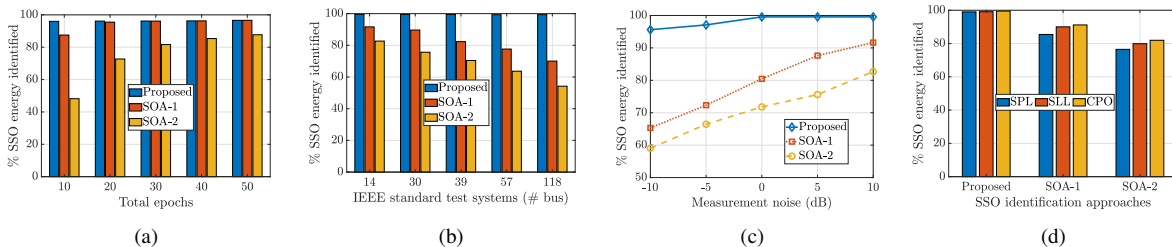
Fig. 4: *% SSO energy captured versus (a) total number of epochs (run-time) for a single power system node, (b) for a complete power network with increasing number of nodes, (c) in a power network with noise in the measurement data, and (d) grid or PMU adversities in IEEE 14-bus test system; CPO: compromised PMU operation, SOA-1: [39], SOA-2: [8].*

compromised PMU operation. However, since a collective analysis of the PMU data is undertaken in the proposed methodology, the execution time does not increases significantly. On closer inspection, we note an average % increment of $\approx 36\%$ in the execution time corresponding to various IEEE test networks, considering cyber attacks. In conclusion, the proposed optimization formulation, based on the co-analysis of data from multiple PMUs, can detect network oscillations using data with measurement noise and while considering cyber attacks on the PMU, while capturing a sufficient energy band of the disturbance wave and in sufficiently less time compared to the state-of-the-art.

F. Comparison wrt the State-of-the-Art Approaches

In this subsection, we conduct a detailed comparative analysis with two diverse SSO identification approaches from the state-of-the-art (SOA). SOA-1 [39] uses a machine learning approach while SOA-2 [8] uses a statistical approach. The comparison outlines the % SSO energy captured as a function of variables such as, total run epochs for one power network node, different system sizes (nodes/buses), measurement noise in dB, and various grid/PMU adversities.

From Fig. 4(a) we observe that, in the detection of oscillations at the node level, both the proposed approach and SOA-1

reach similar detection accuracy, with the proposed approach attaining the maximum efficiency ($\approx 96\%$) in ≈ 10 detection epochs. The requirement of higher time order in SOA-1 is attributed to the involved training and testing phases. Also, the PMU data-based statistical oscillation identification strategy in SOA-2 renders lesser efficiency as they do not utilize inter-attribute correlation in the multivariate dataset.

Next, from Fig. 4(b) we note that the proposed approach outperforms SOA-1 (18.89% better) and SOA-2 (31.654% better) in identifying SSOs in a complete power grid ($\approx 25\%$ better on average). Furthermore, the performance of the state-of-the-art approaches degrade with the increase in the system size (efficiency drop per unit increase in system node $\Delta\eta$: $\Delta\eta_{\text{SOA}-1} = 20.77\%$, $\Delta\eta_{\text{SOA}-2} = 27.37\%$), while the proposed approach performs similarly for systems of varied sizes ($\Delta\eta_{\text{Proposed}} = 0.21\%$). This performance loss is attributed to the missing aspect of co-analysis of data from multiple PMUs, which is a key proposition in our SSO identification approach.

From Fig. 4(c) we observe the performance deterioration resulting from the use of noisy PMU dataset (20.57% in SOA-1 and 27.96% in SOA-2 on an average, i.e., $\approx 25\%$ enhanced noise immunity on average), which is taken care by the noise-resistant oscillation identification approach proposed in this work (c.f. Section IV-C). Also, from Fig. 4(d) it is notable

that, the co-analysis strategy proposed in our approach makes the proposed oscillation detection framework immune to grid adversities arising from single line loss (SLL), communication or hardware failure resulting in single PMU loss (SPL), and compromised PMU operation. The proposed approach demonstrates 10.33% and 19.78% increased efficiency ($\approx 15\%$ enhanced immunity to grid adversities on average) compared to SOA-1 and SOA-2, respectively.

VI. Concluding Remarks

Identification of SSOs in the modern power networks is a crucial task for their reliable operation. This paper conducted a benchmark analysis on identifying the most qualified buses that can help in characterizing the disturbance profile of the entire power network. The proposed approach offers a reduced time complexity compared to the classical approaches and it does not have the model complexity as in the learning-based approaches. For this purpose, an optimization problem was formulated for the theoretical characterization of such nodes, with sole reliance on the small signal modeling of the power networks. A data-driven optimization was formulated, utilizing PMU data obtained from RSCAD simulation, which corroborated the results from the initial theoretical characterization. As a consequence, the most qualified node selection optimization translates to the selection of the most qualified PMUs, the data from which can be co-analyzed to capture a significant fraction of energy in the power network SSOs.

Real PMU data monitoring scenarios with measurement noise-infested data measurements was considered and a mathematical treatment of the measurement noise-infested PMU data was suggested. Other practical system scenarios, such as single PMU loss, single line loss, and compromised PMU operation were simulated and the optimization problem was solved. An intermediate result for the most critical feature of the grid was noted, signifying the grid feature with the highest mutual information about the disturbances in the network. The solution to the optimization problems demonstrated that, by selecting the most qualified buses, the disturbance profile for the entire power network can be gathered in a reduced time frame while capturing a considerable fraction of the total energy in the disturbance wave. The results were validated for various standard IEEE test systems, under various measurement noise profile, and system adversities. The comparison of the proposed algorithm with the state-of-the-art ML and statistical SSO identifiers proves its enhanced abilities in efficiently identifying SSOs in power networks of various sizes, under different adversities and measurement noise considerations.

Appendix

A. Proof of Lemma 1

Given SVD of $\mathbf{D} = \mathbf{U}\boldsymbol{\Sigma}\mathbf{V}^T$, let $\mathbf{D} = \hat{\mathbf{U}}\hat{\boldsymbol{\Sigma}}\hat{\mathbf{V}}^T$, we suppose $\hat{\mathbf{U}} = \mathbf{PU}$, $\hat{\mathbf{V}} = \mathbf{QV}$, and $\hat{\boldsymbol{\Sigma}} = \boldsymbol{\Sigma} + \boldsymbol{\Delta}$, s.t. the singular values are absolutely bounded as $|\sigma_i - \hat{\sigma}_i| \leq \|\mathbf{E}\|_F$, where $\|\cdot\|_F$ denotes the Forbenius norm. Since the error $\mathbf{E}$ is small, it is fair to assume that the rotation in the respective eigenspaces is small. As a consequence, the rotations can be approximated

as $\mathbf{P} = \mathbf{I} + \mathbf{dP}$ and $\mathbf{Q} = \mathbf{I} + \mathbf{dQ}$, respectively, where $\mathbf{dP}$ and $\mathbf{dQ}$ are small rotational gains. On substituting and comparing both sides in the SVD of $\hat{\mathbf{D}}$, we obtain

$$\mathbf{D} + \mathbf{E} = \mathbf{PDQ}^T + \mathbf{PMQ}^T. \tag{A1}$$

Comparing like terms: $\mathbf{D} = \mathbf{PDQ}^T$ and $\mathbf{E} = \mathbf{PMQ}^T$. On further simplifications, neglecting higher order terms, we get

$$\mathbf{DdQ}^T + \mathbf{dPD} = \mathbf{0} \ \& \ \mathbf{MdQ}^T + \mathbf{dPM} = \mathbf{E} - \mathbf{M}. \tag{A2}$$

On solving mutually (A2), we get

$$\begin{aligned} (\mathbf{M}^T\mathbf{M})^{-1}\mathbf{M}^T\mathbf{PM} - (\mathbf{D}^T\mathbf{D})^{-1}\mathbf{D}^T\mathbf{PD} \\ = (\mathbf{M}^T\mathbf{M})^{-1}\mathbf{M}^T\mathbf{E} - \mathbf{I} \end{aligned} \tag{A3}$$

and $\mathbf{dQ}$ can be derived as $\mathbf{dQ}^T = -(\mathbf{D}^T\mathbf{D})^{-1}\mathbf{D}^T\mathbf{dPD}$. Therefore, finally on substituting the above relations in the SVD of $\hat{\mathbf{D}}$, we obtain

$$\begin{aligned} \hat{\mathbf{D}} =& \mathbf{PU}(\boldsymbol{\Sigma} + \boldsymbol{\Delta})\mathbf{V}^T(\mathbf{I} + \mathbf{dQ})^T \\ =& \mathbf{PU}(\boldsymbol{\Sigma} + \boldsymbol{\Delta})\mathbf{V}^T\left[\mathbf{I} - (\mathbf{D}^T\mathbf{D})^{-1}\mathbf{D}^T\mathbf{dPD}\right]. \end{aligned} \tag{A4}$$

Re-substituting $\mathbf{dP} = \mathbf{P} - \mathbf{I}$ in (A4), the final spectral decomposition is obtained as follows

$$\begin{aligned} \hat{\mathbf{D}} =& \mathbf{PU}(\boldsymbol{\Sigma} + \boldsymbol{\Delta})\mathbf{V}^T(\mathbf{I} + \mathbf{dQ})^T \\ =& \mathbf{PU}(\boldsymbol{\Sigma} + \boldsymbol{\Delta})\mathbf{V}^T\left[2\mathbf{I} - (\mathbf{D}^T\mathbf{D})^{-1}\mathbf{D}^T\mathbf{PD}\right]. \end{aligned} \tag{A5}$$

B. Proof of Lemma 2

We start by simplifying (A3) to determine an approximate solution for $\mathbf{P}$. It is noteworthy that the entries of matrix $\mathbf{M}$ are significantly smaller than that of $\mathbf{D}$. Therefore, we neglect the first term of (A3) to obtain

$$\mathbf{P} = \mathbf{I} - \mathbf{D}\left(\mathbf{M}^T\mathbf{M}\right)^{-1}\mathbf{M}^T\mathbf{ED}^T\left(\mathbf{DD}^T\right)^{-1}. \tag{B1}$$

Here, we evaluate a few important moments of $\mathbf{P}$, as follows

$$\begin{aligned} \mathbb{E}[\mathbf{P}] =& \mathbf{I} - \mathbf{D}\left(\mathbf{M}^T\mathbf{M}\right)^{-1}\mathbf{M}^T\mathbb{E}[\mathbf{E}]\mathbf{D}^T\left(\mathbf{DD}^T\right)^{-1} = \mathbf{I} \\ \mathbb{E}[\mathbf{P}^T\mathbf{E}_{ij}] =& \mathbb{E}[(\mathbf{I} - (\mathbf{DD}^T)^{-1}\mathbf{DE}^T\mathbf{M}(\mathbf{M}^T\mathbf{M})^{-1}\mathbf{D}^T)\mathbf{E}_{ij}] \\ =& -(\mathbf{DD}^T)^{-1}\mathbf{DQ}_0 \\ \mathbb{E}[\mathbf{P}^T\mathbf{P}] =& \mathbf{I} + (\mathbf{DD}^T)^{-1}\mathbf{DQ}_1\mathbf{D}^T(\mathbf{DD}^T)^{-1}, \end{aligned}$$

where $\mathbf{Q}_0 = \mathbb{E}[\mathbf{E}^T\mathbf{M}(\mathbf{M}^T\mathbf{M})^{-1}\mathbf{D}^T\mathbf{E}_{ij}]$, $\mathbf{Q}_1 = \mathbb{E}[(\mathbf{ZE})^T(\mathbf{ZE})]$, and $\mathbf{Z} = \mathbf{D}(\mathbf{M}^T\mathbf{M})^{-1}\mathbf{M}^T$. Therefore, the correlation defined in (11) is re-calculated as follows

$$\hat{\rho}_{ij}^{(m)} = \hat{\rho}\left(\hat{\mathbf{u}}_m, \hat{\mathbf{R}}_{ij}\right) = \mathbb{E}[\hat{\mathbf{u}}_m^T\hat{\mathbf{R}}_{ij}]/\hat{\sigma}_{\hat{\mathbf{u}}_m}\hat{\sigma}_{\hat{\mathbf{R}}_{ij}} = \rho_N/\rho_D. \tag{B2}$$

Therefore, evaluating the numerator and denominator terms separately, we get the numerator as

$$\begin{aligned} \rho_N =& \mathbb{E}[(\mathbf{Pu}_m - \mathbb{E}[\mathbf{Pu}_m])^T(\tilde{\mathbf{R}}_{ij} + \mathbf{E}_{ij})] \\ =& \mathbb{E}[(\mathbf{Pu}_m - \mathbf{P}\mu_{\mathbf{u}_m})^T(\tilde{\mathbf{R}}_{ij} + \mathbf{E}_{ij})] \\ =& \mathbb{E}[\tilde{\mathbf{u}}_m^T\tilde{\mathbf{R}}_{ij}] + \mathbf{u}_m^T\mathbb{E}[\mathbf{P}^T\mathbf{E}_{ij}] = \mathbb{E}[\tilde{\mathbf{u}}_m^T\tilde{\mathbf{R}}_{ij}] - (\mathbf{DD}^T)^{-1}\mathbf{DQ}_0. \end{aligned}$$

Similarly, the denominator is evaluated in (B3). For the additive terms, it is fair to assume that the ratios are $\ll 1$, as the measurement error in a well-made device cannot be comparable to the actual measurements. Therefore, the term

$$\rho_D = \sqrt{\mathbb{E}[(\mathbf{u}_m - \mu_{\mathbf{u}_m})^T \mathbf{P}^T \mathbf{P}(\mathbf{u}_m - \mu_{\mathbf{u}_m})] \mathbb{E}[(\tilde{\mathbf{R}}_{ij} + \mathbf{E}_{ij})^T (\tilde{\mathbf{R}}_{ij} + \mathbf{E}_{ij})]} = \sqrt{\left(\sigma_{\tilde{\mathbf{u}}_m}^2 + \mathbf{u}_m^T (\mathbb{E}[\mathbf{P}^T \mathbf{P}] - \mathbf{I}) \mathbf{u}_m \right) \left(\sigma_{\tilde{\mathbf{R}}_{ij}}^2 + \mathbb{E}[\mathbf{E}_{ij}^T \mathbf{E}_{ij}] \right)}$$

$$= \sigma_{\tilde{\mathbf{u}}_m} \sigma_{\tilde{\mathbf{R}}_{ij}} \sqrt{\left(1 + \mathbf{u}_m^T (\mathbf{DD}^T)^{-1} \mathbf{DQ}_1 \mathbf{D}^T (\mathbf{DD}^T)^{-1} \mathbf{u}_m / \sigma_{\tilde{\mathbf{u}}_m}^2 \right) \left(1 + \mathbb{E}[\mathbf{E}_{ij}^T \mathbf{E}_{ij}] / \sigma_{\tilde{\mathbf{R}}_{ij}}^2 \right)}. \qquad \text{(B3)}$$

inside the root can be approximated as follows

$$\rho_D = \sigma_{\tilde{\mathbf{u}}_m} \sigma_{\tilde{\mathbf{R}}_{ij}} + \frac{\mathbf{u}_m^T (\mathbf{DD}^T)^{-1} \mathbf{DQ}_1 \mathbf{D}^T (\mathbf{DD}^T)^{-1} \mathbf{u}_m}{2 \sigma_{\tilde{\mathbf{u}}_m} / \sigma_{\tilde{\mathbf{R}}_{ij}}} + \frac{\mathbb{E}[\mathbf{E}_{ij}^T \mathbf{E}_{ij}]}{2 \sigma_{\tilde{\mathbf{R}}_{ij}} / \sigma_{\tilde{\mathbf{u}}_m}}.$$

Therefore, $\hat{\rho}_{ij}^{(m)} = \rho_{ij}^{(m)} \left(\frac{1 - \zeta_1}{1 + \zeta_2} \right)$, where $\zeta_1 = \frac{(\mathbf{DD}^T)^{-1} \mathbf{DQ}_0}{\mathbb{E}[\tilde{\mathbf{u}}_m^T \tilde{\mathbf{R}}_{ij}]}$
and $\zeta_2 = \frac{\mathbf{u}_m^T (\mathbf{DD}^T)^{-1} \mathbf{DQ}_1 \mathbf{D}^T (\mathbf{DD}^T)^{-1} \mathbf{u}_m}{2 \sigma_{\tilde{\mathbf{u}}_m}^2} + \frac{\mathbb{E}[\mathbf{E}_{ij}^T \mathbf{E}_{ij}]}{2 \sigma_{\tilde{\mathbf{R}}_{ij}}^2}$.

C. Proof of Lemma 3

We start by taking Fourier transform of the jth column of the ith PMU dataset impaired by measurement noise given by

$$\hat{\mathfrak{R}}_{ij} = \mathcal{F}\left(\hat{\mathbf{R}}_{ij} \right) = \mathcal{F}\left(\tilde{\mathbf{R}}_{ij} \right) + \mathcal{F}\left(\mathbf{E}_{ij} \right) = \mathfrak{R}_{ij} + \partial \mathfrak{R}_{ij}$$

where $\partial \mathfrak{R}_{ij} = \mathcal{F}\left(\mathbf{E}_{ij} \right)$ is the Fourier spectrum of the measurement noise. Therefore, the revised conditional for hypothesis 4 can be obtained as

$$\hat{\mathfrak{P}}_{ij} = \frac{\mathfrak{K}\left(\hat{\mathfrak{R}}_{ij} \right)}{\| \mathfrak{K}\left(\mathfrak{R}_{ij} \right) \|_c} = \frac{\mathfrak{K}\left(\mathfrak{R}_{ij} + \partial \mathfrak{R}_{ij} \right)}{\| \mathfrak{K}\left(\mathfrak{R}_{ij} \right) \|_c}. \qquad \text{(C1)}$$

Applying triangle inequality in (C1), we get

$$\hat{\mathfrak{P}}_{ij} \leq \frac{\mathfrak{K}\left(\mathfrak{R}_{ij} \right) + \mathfrak{K}\left(\partial \mathfrak{R}_{ij} \right)}{\| \mathfrak{K}\left(\hat{\mathfrak{R}}_{ij} \right) \|_c} \leq \mathfrak{P}_{ij} + \frac{\mathfrak{K}\left(\partial \mathfrak{R}_{ij} \right)}{\| \mathfrak{K}\left(\mathfrak{R}_{ij} \right) \|_c}. \qquad \text{(C2)}$$

Motivated by (C2), we revise the hypothesis threshold to $\mathfrak{P}_{\text{th}} \rightarrow \mathfrak{P}_{\text{th}} + \frac{\mathfrak{K}(\partial \mathfrak{R}_{ij})}{\| \mathfrak{K}(\mathfrak{R}_{ij}) \|_c}$. Consequently, the revised $b_i^{(f)}$ is restored to its previous value.

REFERENCES

[1] Q. Hou, E. Du, N. Zhang, and C. Kang, "Impact of high renewable penetration on the power system operation mode: A data-driven approach," *IEEE Trans. Power Syst.*, vol. 35, no. 1, pp. 731–741, 2019.

[2] W. Du, B. Ren, H. Wang, and Y. Wang, "Comparison of methods to examine sub-synchronous oscillations caused by grid-connected wind turbine generators," *IEEE Trans. Power Syst.*, vol. 34, no. 6, pp. 4931–4943, 2019.

[3] A. K. Mandal, A. Malkhandi, S. De, N. Senroy, and S. Mishra, "A multipath model for disturbance propagation in electrical power networks," *IEEE Trans. Circuits Syst. II: Express Briefs*, vol. 70, no. 4, pp. 1460–1464, 2022.

[4] Z. Li, H. Liu, J. Zhao, T. Bi, and Q. Yang, "A power system disturbance classification method robust to PMU data quality issues," *IEEE Trans. Indus. Informat.*, vol. 18, no. 1, pp. 130–142, 2021.

[5] R. Ma, S. Basumallik, and S. Eftekharnejad, "A PMU-based data-driven approach for classifying power system events considering cyberattacks," *IEEE Syst. J.*, vol. 14, no. 3, pp. 3558–3569, 2020.

[6] X. Yang, J. Zhang, X. Xie, X. Xiao, B. Gao, and Y. Wang, "Interpolated DFT-based identification of sub-synchronous oscillation parameters using synchrophasor data," *IEEE Trans. Smart Grid*, vol. 11, no. 3, pp. 2662–2675, 2019.

[7] P. G. Estevez, P. Marchi, F. Messina, and C. Galarza, "Forced oscillation identification and filtering from multi-channel time-frequency representation," *IEEE Trans. Power Syst.*, vol. 36, no. 2, pp. 1257–1269, 2020.

[8] F. Zhang, L. Cheng, W. Gao, and R. Huang, "Synchrophasors-based identification for subsynchronous oscillations in power systems," *IEEE Trans. Smart Grid*, vol. 10, no. 2, pp. 2224–2233, 2018.

[9] F. Zhang, J. Li, J. Liu, W. Gao, and J. He, "An improved interpolated DFT-based parameter identification for sub-/super-synchronous oscillations with synchrophasors," *IEEE Trans. Power Syst.*, vol. 38, no. 2, pp. 1714–1727, 2022.

[10] E. Sezgin and Ö. Salor, "Analysis of power system harmonic subgroups of the electric arc furnace currents based on a hybrid time-frequency analysis method," *IEEE Trans. Indus. Appl.*, vol. 55, no. 4, pp. 4398–4406, 2019.

[11] T. Xia, Z. Yu, K. Sun, D. Shi, and Z. Wang, "Extended prony analysis on power system oscillation under a near-resonance condition," in *in Proc. IEEE Power Energy Society General Meeting (PESGM)*. IEEE, 2020, pp. 1–5.

[12] L. Chen, W. Zhao, F. Wang, Q. Wang, and S. Huang, "An interharmonic phasor and frequency estimator for subsynchronous oscillation identification and monitoring," *IEEE Trans. Instrum. Meas.*, vol. 68, no. 6, pp. 1714–1723, 2018.

[13] B. Gao, R. Torquato, W. Xu, and W. Freitas, "Waveform-based method for fast and accurate identification of subsynchronous resonance events," *IEEE Trans. Power Syst.*, vol. 34, no. 5, pp. 3626–3636, 2019.

[14] J. G. Philip, J. Jung, and A. Onen, "Empirical wavelet transform based method for identification and analysis of sub-synchronous oscillation modes using PMU data," *J. Modern Power Syst. Clean Ener.*, 2023.

[15] X. Xie, Y. Zhan, H. Liu, W. Li, and C. Wu, "Wide-area monitoring and early-warning of subsynchronous oscillation in power systems with high-penetration of renewables," *Int. J. Elec. Power Ener. Syst.*, vol. 108, pp. 31–39, 2019.

[16] L. G. Meegahapola, S. Bu, D. P. Wadduwage, C. Y. Chung, and X. Yu, "Review on oscillatory stability in power grids with renewable energy sources: Monitoring, analysis, and control using synchrophasor technology," *IEEE Trans. Indus. Electron.*, vol. 68, no. 1, pp. 519–531, 2020.

[17] G. Cheng, Y. Lin, A. Abur, A. Gómez-Expósito, and W. Wu, "A survey of power system state estimation using multiple data sources: Pmus, scada, ami, and beyond," *IEEE Trans. Smart Grid*, 2023.

[18] L. Chu, R. Qiu, X. He, Z. Ling, and Y. Liu, "Massive streaming PMU data modelling and analytics in smart grid state evaluation based on multiple high-dimensional covariance test," *IEEE Trans. Big Data*, vol. 4, no. 1, pp. 55–64, 2017.

[19] W. Xiong, L. Wang, R. Wu, Y. Qi, H. Liu, and T. Bi, "Decision tree based subsynchronous oscillation detection and alarm method using phasor measurement units," in *2020 IEEE Sus. Power Ener. Conf. (iSPEC)*. IEEE, 2020, pp. 2448–2453.

[20] N. Severoglu and Ö. Salor, "Statistical models of EAF harmonics developed for harmonic estimation directly from waveform samples using deep learning framework," *IEEE Trans. Indus. Appl.*, vol. 57, no. 6, pp. 6730–6740, 2021.

[21] Y. Deng, L. Wang, H. Jia, X. Tong, and F. Li, "A sequence-to-sequence deep learning architecture based on bidirectional GRU for type recognition and time location of combined power quality disturbance," *IEEE Trans. Indus. Informat.*, vol. 15, no. 8, pp. 4481–4493, 2019.

[22] F. Liu, S. Lin, J. Ma, and Y. Li, "Data-driven mode identification method for broad-band oscillation of interconnected power system," *IEEE Sensors J.*, vol. 22, no. 15, pp. 15273–15283, 2022.

[23] Y. Wang, W. Min, M. Chao, Y. Liu, and X. Yang, "A data-driven method for SSCI identification using synchrophasor measurements," *Int. J. Elec. Power Ener. Syst.*, vol. 153, p. 109282, 2023.

[24] T. Lan, Y. Lin, J. Wang, B. Leao, and D. Fradkin, "Unsupervised power system event detection and classification using unlabeled PMU data," in *2021 IEEE PES Innov. Smart Grid Technol. Europe (ISGT Europe)*. IEEE, 2021, pp. 01–05.

[25] H. Zhao, J. Liu, H. Chen, J. Chen, Y. Li, J. Xu, and W. Deng, "Intelligent diagnosis using continuous wavelet transform and gauss convolutional deep belief network," *IEEE Trans. Reliability*, 2022.

[26] P. K. Ray, S. R. Mohanty, N. Kishor, and J. P. Catalão, "Optimal feature and decision tree-based classification of power quality disturbances in distributed generation systems," *IEEE Trans. Sustain. Energy*, vol. 5, no. 1, pp. 200–208, 2013.

[27] A. Shahsavari, M. Farajollahi, E. M. Stewart, E. Cortez, and H. Mohsenian-Rad, "Situational awareness in distribution grid using micro-PMU data: A machine learning approach," *IEEE Trans. Smart Grid*, vol. 10, no. 6, pp. 6167–6177, 2019.

[28] K. Chen, J. Hu, and J. He, "A framework for automatically extracting overvoltage features based on sparse autoencoder," *IEEE Trans. Smart Grid*, vol. 9, no. 2, pp. 594–604, 2016.

[29] M. Sahani and P. K. Dash, "Automatic power quality events recognition based on Hilbert Huang transform and weighted bidirectional extreme learning machine," *IEEE Trans. Indus. Informat.*, vol. 14, no. 9, pp. 3849–3858, 2018.

[30] M. I. Jordan and T. M. Mitchell, "Machine learning: Trends, perspectives, and prospects," *Science*, vol. 349, no. 6245, pp. 255–260, 2015.

[31] L. Rice, E. Wong, and Z. Kolter, "Overfitting in adversarially robust deep learning," in *Proc. Int. Conf. Machine Learning*. PMLR, 2020, pp. 8093–8104.

[32] S. Ghosh, A. K. Mandal, S. De, S. Chatterjee, and M. Portmann, "Light-weight ML aided autonomous IoT networks," *IEEE Comm. Mag.*, vol. 61, no. 6, pp. 51–57, 2023.

[33] Z. Li, H. Liu, J. Zhao, T. Bi, and Q. Yang, "A power system disturbance classification method robust to PMU data quality issues," *IEEE Trans. Indus. Informat.*, vol. 18, no. 1, pp. 130–142, 2022.

[34] A. K. Mandal and S. De, "Characterization of qualified grid nodes for the identification of power network oscillations," in *Proc. IEEE Int. Conf. Ener. Technol. Future Grids (ETFG)*. IEEE, 2023, pp. 1–6.

[35] Z. S. Khalafi, M. Dehghani, A. Khalili, A. Sami, N. Vafamand, and T. Dragičević, "Intrusion detection, measurement correction, and attack localization of PMU networks," *IEEE Tran. Indus. Electron.*, vol. 69, no. 5, pp. 4697–4706, 2021.

[36] G. Frigo, A. Derviškadić, A. Bach, and M. Paolone, "Statistical model of measurement noise in real-world PMU-based acquisitions," in *Proc. Int. Conf. Smart Grid Sync. Meas. Ana. (SGSMA)*. IEEE, 2019, pp. 1–8.

[37] M. Z. H. El-Din, "An efficient approach for dynamic stability analysis of power systems-including load effects," Ph.D. dissertation, 1977.

[38] M. Shafiullah, M. I. Hossain, M. Abido, T. Abdel-Fattah, and A. Mantawy, "A modified optimal PMU placement problem formulation considering channel limits under various contingencies," *Measurement*, vol. 135, pp. 875–885, 2019.

[39] S. Liu, S. You, Z. Lin, C. Zeng, H. Li, W. Wang, X. Hu, and Y. Liu, "Data-driven event identification in the US power systems based on 2D-OLPP and RUSBoosted trees," *IEEE Trans. Power Syst.*, vol. 37, no. 1, pp. 94–105, 2021.